Polyaniline–Cobalt Hexacyanoferrate Composites as High-Performance Cathodes for Zn-Ion Hybrid Supercapacitor

Yiyang Liu, Xueying Hu, Hongzhen He, Jianwei Li, Haobo Dong, Paul R. Shearing, Guanjie He,* and Dan J. L. Brett*

Zn-based hybrid supercapacitors (ZHSCs) have received increasing attention in recent research, due to their high electrochemical performance and low cost. Herein, a composite cathode is developed based on polyaniline (PANI) and cobalt hexacyanoferrate (CoHCF), exhibiting excellent electrochemical performance. The results showed that PANI is coated on CoHCF, thereby enhancing the electrical conductivity and Zn^{2+} transport kinetics. As a result, the as-prepared materials demonstrate remarkable specific capacitance (741.7 F g^{-1} at 5 mV s^{-1}), good cycling durability (86.15% capacitance retention over 5000 cycles at 10 A g^{-1}), high peak energy density (312 Wh kg^{-1} at 500 W kg^{-1}), and superior power density (75 294 W kg^{-1} at 25 Wh kg^{-1}). The excellent electrochemical performance confirms that PANI–CoHCF composites are promising cathode candidates for ZHSCs in practical applications.

1. Introduction

The steadily advancing electrification process puts forward new demands for next-generation electrochemical energy storage (EES) devices, which require EES devices to possess high energy density, high power density, high safety, and low cost

Y. Liu, H. He, P. R. Shearing, G. He, D. J. L. Brett
Electrochemical Innovation Lab (EIL)
Department of Chemical Engineering
University College London (UCL)
London WC1E 7JE, UK
E-mail: g.he@ucl.ac.uk; d.brett@ucl.ac.uk

Y. Liu, X. Hu, H. He, J. Li, H. Dong, G. He
Christopher Ingold Laboratory
Department of Chemistry
University College London (UCL)
London WC1H 0AJ, UK

P. R. Shearing, D. J. L. Brett
The Faraday Institution
Quad One
Harwell Campus, Didcot OX11 0RA, UK

The ORCID identification number(s) for the author(s) of this article can be found under https://doi.org/10.1002/ente.202201368.

simultaneously.[1,2] Although lithium-ion batteries (LIBs) have shown their advantages in energy density (100–265 Wh kg^{-1}) and dominate the current rechargeable EES market, they still face some challenges, such as high cost (>\$100 per kWh) and limited raw material reserve.[3] In addition, the use of organic electrolytes with weak ionic conductivity ($\approx 10^{-3}$ S cm^{-1}) limits the power density of LIBs (100–300 W kg^{-1}), making it difficult for LIBs to be used in scenarios with high power requirements.[4] On the contrary, aqueous electrolytes deliver a higher ionic conductivity (≈ 1 S cm^{-1}), which lays the foundation for achieving high power density.[5,6]

Conventional electric double-layer capacitors (EDLCs) and pseudocapacitors are promising candidates for achieving high power density, which can usually reach power densities above 10 kW kg^{-1}; however, they can only reach an energy density below 10 Wh kg^{-1}, which retards their practical employment.[7,8] Zn-ion hybrid supercapacitors (ZHSCs) are emerging EES technologies proposed in recent years, which couple battery-type anodes (reversible electrodeposition and dissolution of Zn metal) and capacitor-type cathodes (EDLC or pseudocapacitors).[9,10] Following the concept of combining two different types of electrodes with battery-type Faradic electrode and capacitor-type electrode, respectively,[11,12] Mai et al have proved that the preintercalated method can increase the lattice distance facilitating the Zn2+ intercalation mechanism and result in a high areal energy density and power density.[13,14] ZHSCs are expected to integrate both features of batteries and capacitors, that is, they could achieve high specific capacity (820 mAh g^{-1} Zn), good energy density (1353 Wh kg^{-1} Zn), high power density, and long durability.[15] However, current ZHSCs still cannot achieve ideal electrochemical performances. This is because the specific capacitance of the state-of-the-art cathode materials is limited (typically 150–400 F g^{-1}), which cannot match the high theoretical capacity of Zn anodes, thus resulting in the low utilization rate of the Zn anode.[16,17]

In addition to other electrode materials such as carbon materials and metal oxides (e.g., RuO_2 and MnO_2), conductive polymers are promising pseudocapacitive materials, achieving high specific capacitance through rapid surface redox reactions.[18] Among them, polyaniline (PANI) is one of the most applied candidates, owing to their attractive merits in high specific

capacitance, easy fabrication process, low cost, and environmental friendliness.[19] However, the doping/undoping of charged ions involved in PANI during cycling may cause swelling, shrinkage, and cracking, resulting in poor cycle stability.[20] Moreover, PANI could be intensively oxidized under a high potential, causing degradation of the material, thereby limiting the working potential of the electrode. The channel collapse and electrode swelling during the cycling will dramatically decrease the effective specific surface area, thus deteriorating ion transport kinetics and resulting in rapid capacitance decay after a few cycles.[21] It is essential to stabilize the PANI-based layered structure for further improvement in electrochemical performances.

Prussian blue analogues (PBAs), a type of electrochemically active material with large interstitial sites and channels in the open-framework structures, have been widely exploited in the fields of energy storage, electrocatalysis, sensors, etc.[22–24] The well-constructed structures of PBAs enable a stable charging/discharging performance, which is a supplemental advantage regarding the PANI electrode. In the meantime, PBAs are also promising cathode candidates for ZHSCs because of their high power density, high economic availability, and facile manufacturing processes.[25] However, some inherent shortcomings of PBAs, such as poor electrical conductivity and the dissolution/phase change in aqueous electrolytes, result in sluggish electron transfer kinetics and poor stability, thus limiting their further applications in ZHSC.[4] Hence, in this work, a series of PANI–cobalt hexacyanoferrate (CoHCF) hybrid cathodes were developed for ZHSCs in different compositions combining both merits in cycling stability and high specific capacitance. These PANI–CoHCF demonstrated various favorable synergistic effects in reducing electrical resistance and facilitating ion transport kinetics, thus achieving a high specific capacitance, long durability, and excellent energy/power density.

2. Experimental Section

As illustrated in **Figure 1**, PANI, CoHCF, and a series of PANI–CoHCF composites with different ratios of PANI and CoHCF were synthesized accordingly. The composites were named PANI–CoHCF A–E according to the content of PANI from high to low. Subsequently, the as-prepared active materials were mixed with Super P carbon and polyvinylidene difluoride (PVDF) with a weight ratio of 7:2:1 to form a homogeneous mixture. Next, the mixture was coated on a piece of hydrophilic carbon paper and then dried in a vacuum oven at 70 °C for 24 h. The ZHSCs were assembled in CR2032-type coin cells with a 0.2 mm-thick Zn foil as the anode and 3 M ZnSO4 solution as the aqueous electrolyte under an ambient environment. A series of material characterization and electrochemical tests were conducted. Details of the Experimental Section are provided in the Supporting Information.

3. Results and Discussion

3.1. Material Synthesis and Characterization

The X-ray diffraction (XRD) patterns of PANI, CoHCF, and PANI–CoHCF-D are shown in **Figure 2**a. The diffraction peaks at $2\theta = 7.70°$, 10.95°, 15.68°, 17.60°, 19.28°, 22.36°, 23.72°, and 25.10° correspond to the (200), (220), (400), (420), (422), (440), (600), and (620) lattice planes of CoHCF (ICSD: 97-002-3102), respectively. The highest intensity of the (200) plane reveals that CoHCF has a stable face-centered-cubic (FCC) crystal structure (space group $Fm3(\_)m$). Meanwhile, PANI–CoHCF-A–E (Figure S1c–g, Supporting Information) all have similar characteristic patterns compared to CoHCF, which indicates that the acidic environment does not cause a significant influence on the structure of CoHCF. In addition, with the addition of polyaniline, the diffraction peak of PANI–CoHCF-D becomes narrower than that of pure CoHCF. This reveals that the PANI coating may facilitate the removal of crystal water and increase the crystallinity of CoH.[26]

To further verify the chemical composition of PANI–CoHCF composites, Fourier-transform infrared spectroscopy (FTIR) spectra of pure CoHCF and PANI–CoHCF-D were recorded. As shown in Figure 2b, PANI–CoHCF-D displays eight peaks: 1136, 1240, 1304, 1495, 1582, 2085, 3356, and 3632 cm^{-1}. As illustrated in the FTIR spectra, a characteristic peak at 2085 cm^{-1} is the stretching vibration of $C \equiv N$ in CoHCF.[27] The peaks located at 1495 and 1582 cm^{-1} correspond to the stretching vibrational peaks of benzene and quinone in PANI, respectively.[28] Overall, the peaks at 1000–1600 cm^{-1} are assigned to the C–N structure and benzene ring in PANI–CoHCF-D, which revealed that PANI coating is successfully encapsulated on the surface of CoHCF. Raman spectrum shown in Figure S7, Supporting Information, also reveals the characteristic peaks. Both characteristic groups for PANI of benzene ring and quinone are detected. Function groups in C≡N and C aN are also attained which belong to CoHCF. In terms of the X-ray photoelectron spectroscopy results (see Figure S7, Supporting Information), C–C (284.8 eV), C–N (85.8 eV), and C=O (287.7 eV) correspond to the N—C=O for CoHCF and the C=O bond for PANI. N triple bond at 397.8 eV is attributed to COHCF and PANI structure, and NH bond at 399.1 eV is attributed to PANI. As displayed in **Figure 3**a–c, scanning electron microscope (SEM) images for both pristine and hybrid electrodes exhibit a lumped-shape structure, which is amorphous. In addition, energy-dispersive X-ray spectroscopy (EDS) mapping shown in Figure 3d revealed the uniform distribution of PANI on the CoHCF surface. Besides, compared to pure CoHCF, the peaks at 1601, 3363, and 3632 cm^{-1} become weaker in PANI–CoHCF-D, indicating that the introduction of PANI facilitates the lattice water removal. One possible speculation is that the crystal water inside CoHCF is gradually transferred to PANI through cationic defect sites, thereby constructing more active sites for (de)intercalation and enhancing the diffusion kinetics of Zn^{2+} in the PANI–CoHCF composites. This is consistent with the observation from previous results.[29]

3.2. Electrochemical Performance

A series of electrochemical tests for PANI, CoHCF, and PANI–CoHCF composites were conducted in the coin cell configuration. The cyclic voltammetry (CV) curves (5 Mv s^{-1} scan rate, **Figure 4**a and S4, Supporting Information) of PANI, CoHCF, and PANI–CoHCF composites with various ratios demonstrated the typical redox peaks of PANI and CoHCF.[30,31] For example, it can be seen that the CoHCF electrode displayed a pair of redox
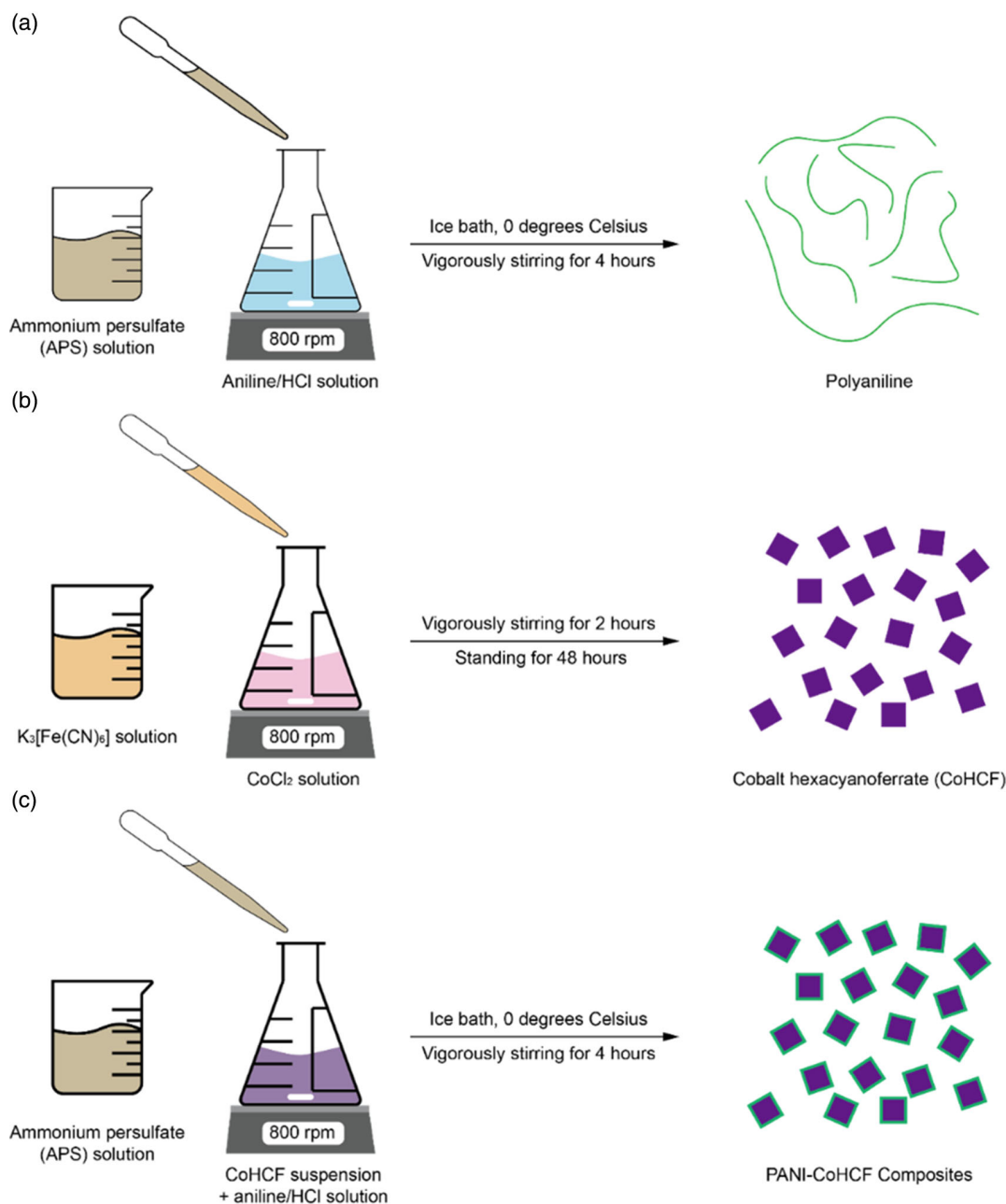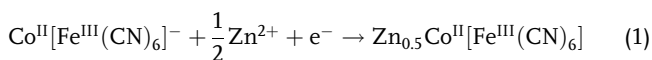
Figure 1. Schematic diagram of the synthesis of a) PANI, b) CoHCF, and c) PANI–CoHCF composites.

peaks at ≈1.9 V/1.73 V, which is attributed to the redox reaction of Fe^{2+}/Fe^{3+} couple coordinated *via* $C \equiv N$ group.

$$Co^{II}[Fe^{III}(CN)_6]^- + \frac{1}{2}Zn^{2+} + e^- \rightarrow Zn_{0.5}Co^{II}[Fe^{III}(CN)_6] \qquad (1)$$

Compared with the CoHCF, all PANI–CoHCF composites exhibited an increase in the peak current, which should be attributed to the 1) improvement of the electrical conductivity and charge storage behaviors of the electrode material by the PANI coating and 2) synergistic effects between the PANI and CoHCF. The specific capacitance of different electrode materials can be roughly estimated by calculating the area enclosed by the CV curves. Compared to PANI, CoHCF only has a minimal specific capacitance. As the mass ratio of PANI increases, the specific capacitance of the PANI–CoHCF complex gradually increases, and the optimal electrochemical activity is achieved in PANI–CoHCF-D. The results revealed that due to lower ion diffusion and electron transport properties, the PANI–CoHCF composite with less PANI coating has a relatively low specific capacitance, while excessive PANI coating will hinder the (de)insertion of Zn^{2+} in CoHCF, thereby reducing the specific capacitance. Therefore, this work chose PANI–CoHCF-D for further research.

Pristine CoHCF only exhibits obvious redox peaks (see Figure S4b, Supporting Information). Hence it is a typical
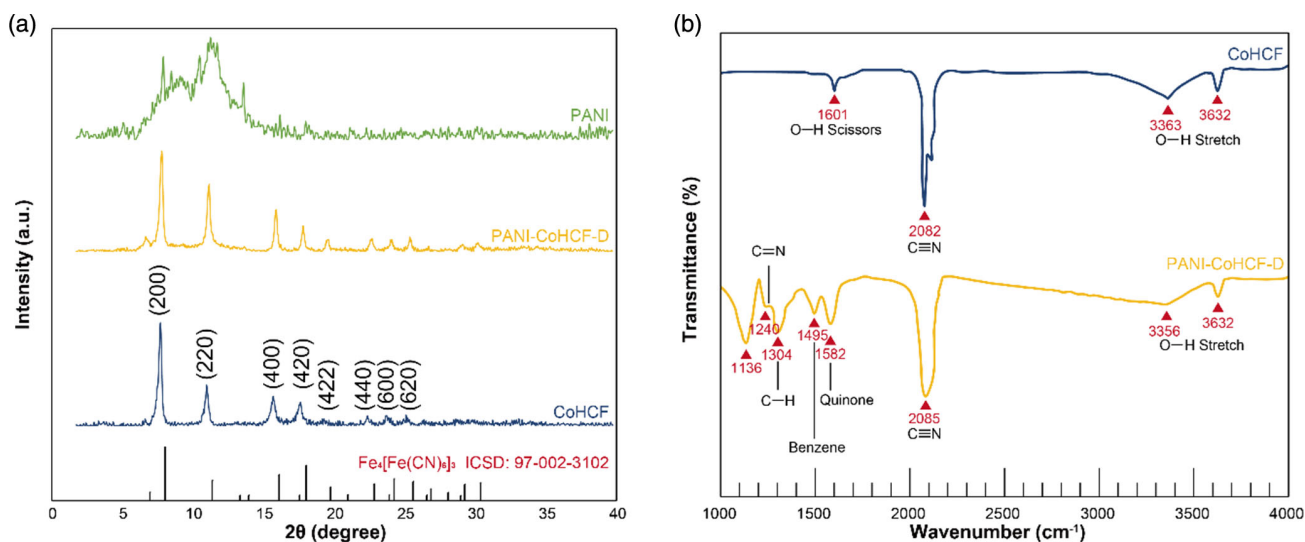
Figure 2. a) XRD spectra of PANI, CoHCF, and PANI–CoHCF-D. b) FTIR spectra of CoHCF and PANI–CoHCF-D.
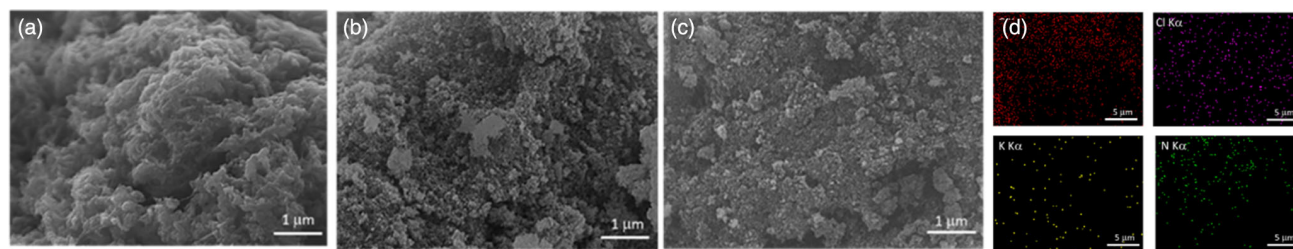

Figure 3. Surface morphology of both pristine and hybrid cathode. a) SEM image for pristine PANI; b) SEM image for pure CoHCF; c) SEM image for hybrid PANI-PB-A; d) EDS images for corresponding PANI-PB-A.

battery-type active material; whereas pristine PANI and PANI–CoHCF composites exhibit more pseudocapacitive characteristics. In particular, PANI–CoHCF-D exhibits a CV curve close to a parallelogram, which is the typical characteristic of the CV curve of a pseudocapacitance-dominated material. For PANI–CoHCF-D, there are two pairs of redox peaks at 1.27 V/0.97 V (corresponding to PANI) and 1.90 V/1.55 V (corresponding to PANI and CoHCF). The PANI–CoHCF-D electrode exhibited obvious symmetric redox peaks, indicating its good capacitive behavior and high reversibility during the Zn^{2+} (de) intercalation. Figure 4b shows the CV curves of the PANI–CoHCF-D electrode measured at different scan rates. As the scan rate increases from 5 to 50 mV s^{-1}, the redox current increases significantly, while the oxidation peak gradually shifts to a positive potential, and the reduction peak gradually shifts to a negative potential. Even at a higher scan rate, the CV shape is well maintained in the selected potential window, which indicates the stability of double-layer capacitance/pseudocapacitance caused by the rapid electron transfer on the surface of the PANI–CoHCF-D electrode.

The electrochemical behavior of each material can be further evaluated by galvanostatic charge/discharge (GCD) curves (Figure 4c and S5, Supporting Information). Generally, depending on the type of material, the GCD curve will present three situations: 1) for an electric double-layer capacitive material,

the obtained GCD curve is "inverted V" shape without any distortion; 2) for a battery-type material represented by CoHCF (Figure S5b, Supporting Information), an obvious charging/discharging platform will appear in the GCD curve; and 3) for a pseudocapacitive material represented by PANI (Figure S5a, Supporting Information) and PANI–CoHCF composites (Figure S5c–g, Supporting Information), a slightly distorted "inverted V"-shaped curve will be observed.[10] Compared with pure PANI, PANI–CoHCF composites exhibit more significant distortion due to the combination of two redox materials. These distortions contribute to additional capacitance, which enables the PANI–CoHCF-D electrode to achieve a high specific capacitance of 741.7 F g^{-1}. In addition, the PANI–CoHCF-D electrode exhibits excellent long-term cycling durability (86.15% capacitance retention after 5000 cycles at 10 A g^{-1}), indicating its high reversibility and structural robustness. The high specific capacitance and good cycling stability can be ascribed to 1) compared with pure PANI, the electrochemical active surface area of PANI coated on the cubic CoHCF surface is increased, and the possibility of pore/channel collapse is reduced; 2) the reduction of lattice water in CoHCF increases active sites of Zn^{2+} (de)insertion and improves the material stability; 3) PANI coating can stabilize the PBA particles from severe structure/phase change by keeping them mechanically surface bounded; and 4) PANI enhanced electrical conductivity and electron transfer.
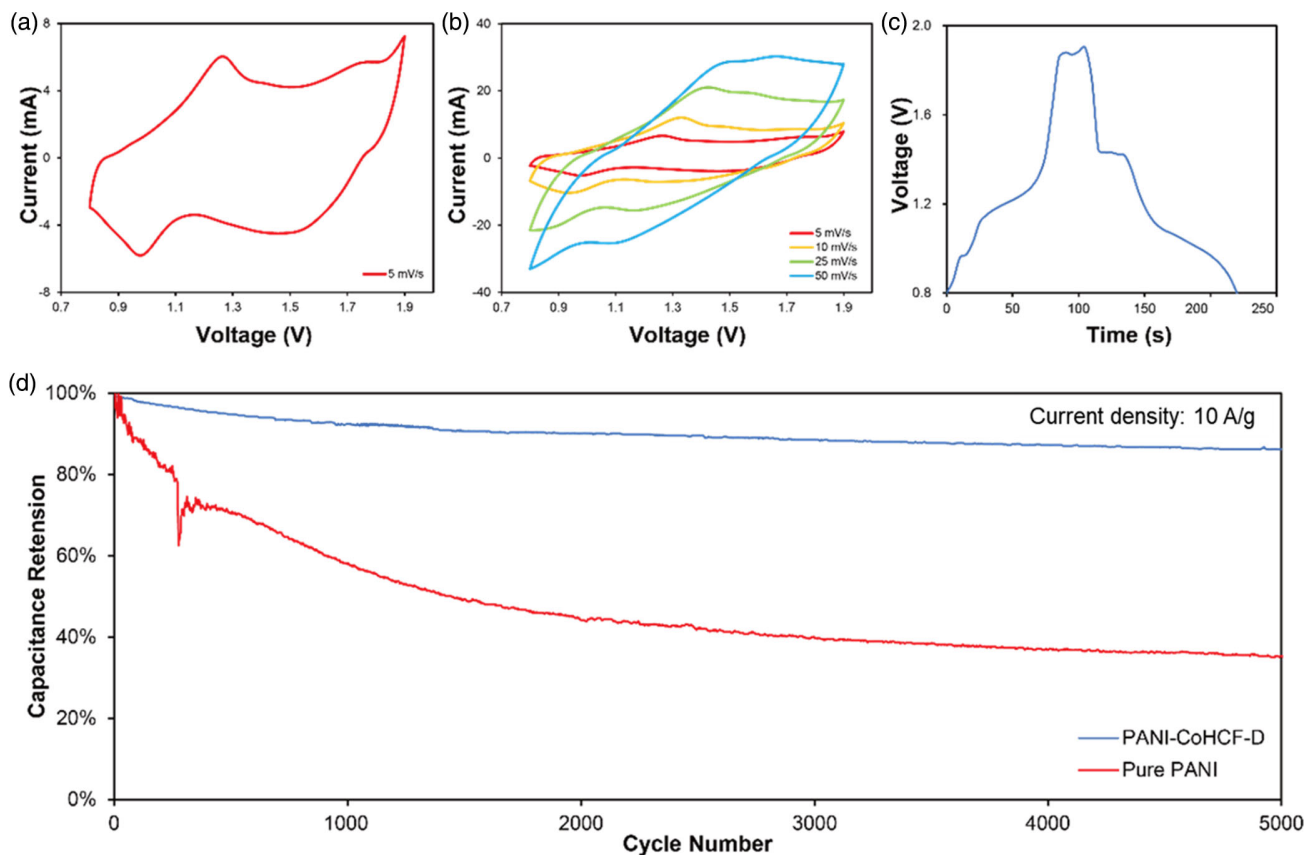
Figure 4. Electrochemical tests of as-assembled Zn-ion hybrid supercapacitors. The CV curve of PANI–CoHCF-D at a) a scan rate of 5 mV s^{-1} and b) different scan rates (5–50 mV s^{-1}); c) GCD curve of PANI–CoHCF-D curve at the current density of 10 A g^{-1}; d) long-term cycling stability of the pure PANI and PANI–CoHCF-D at the current density of 10 A g^{-1}.

Electrochemical impedance spectroscopy (EIS) of PANI, CoHCF, and PANI–CoHCF composites was well investigated under the frequency range from 100 kHz to 100 MHz. It is widely accepted that the first intersection of the semicircle in the high-frequency zone and the Z_{Re} axis represent the equivalent series resistance (R_S) of the ZHSC, which is influenced by the internal resistance of the electrode material, the electrolyte resistance, and the contact resistance between electrode materials and the current collector. As detailed in the Nyquist plot (**Figure 5**), compared with pure CoHCF with low electrical conductivity, the R_S of PANI and PANI–CoHCF is significantly smaller, which confirms the effect of PANI coating on electrical conductivity improvement. Furthermore, R_{CT} corresponds to the charge transfer resistance during the electrochemical measurement process, which could be evaluated by the intersection of the low-frequency end of the semicircular arc and the real axis.[27] Compared with pure PANI and pure CoHCF, all of the PANI–CoHCF composites have lower R_{CT} values, indicating that the synergistic effect of PANI and CoHCF enhances charge transfer kinetics. Among them, PANI–CoHCF-C and D exhibited the lowest R_{CT}, which reveals that the ratio of PANI and CoHCF between the two is the most suitable for constructing an excellent electronic transport framework. In addition, the oblique line in the low-frequency region reflects the Warburg impedance R_W related to Zn^{2+} diffusion at the electrode–electrolyte interface. Compared with other materials,
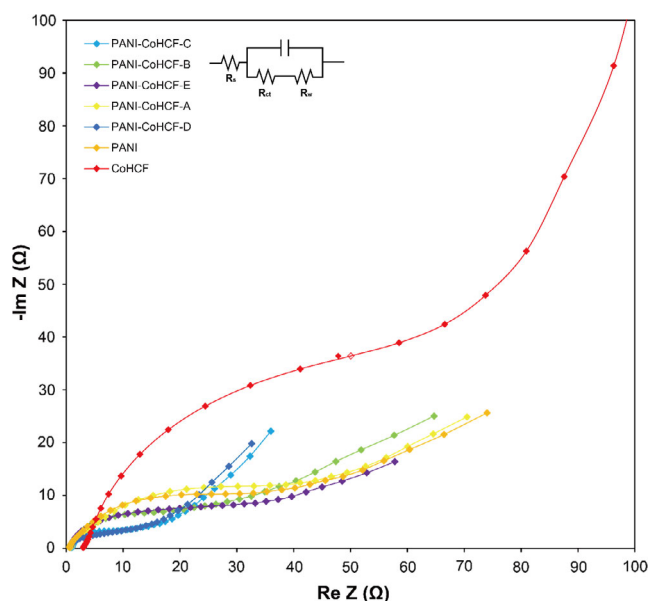

Figure 5. Nyquist plot of PANI, CoHCF, and PANI–CoHCF composites.

the diagonal lines of PANI–CoHCF-C and D are steeper, indicating that they possess better pseudocapacitance performance.
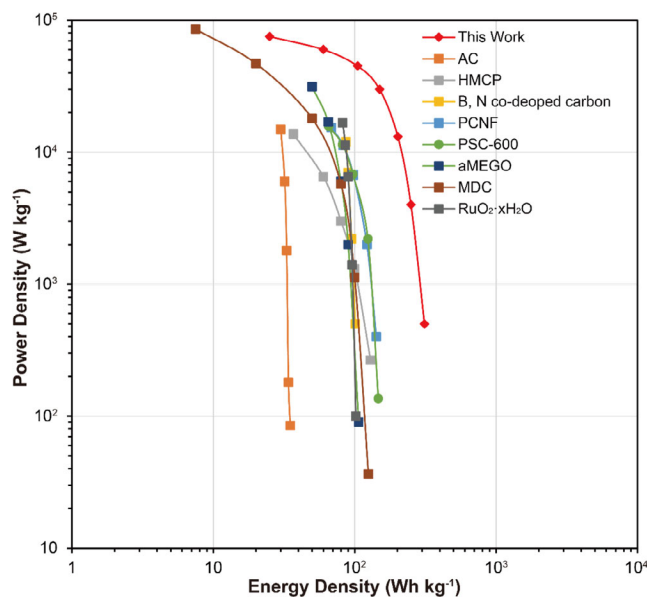
Figure 6. Ragone plot of ZHSCs. The red line is the result delivered in this work.

Based on the coin cell configuration, we also estimated the energy density and power density of PANI–CoHCF-D. Compared with other representative cathode materials for ZHSC (**Figure 6**), the as-prepared material exhibited a remarkable peak power density (75 294 W kg^{-1} at 25 Wh kg^{-1}) and maximum energy density (312 Wh kg^{-1} at 500 W kg^{-1}). Therefore, this material is a promising candidate for ZHSC due to its high energy density, high power density, and extremely low cost.

4. Conclusion

In summary, we have successfully developed PANI–CoHCF composites and optimized their performance by tuning the ratio of PANI and CoHCF. Among them, PANI–CoHCF-D exhibited remarkable specific capacitance (741.7 F g^{-1} at 5 mV s^{-1}), good cycling durability (86.15% capacitance retention over 5000 cycles at 10 A g^{-1}), and excellent energy/power density. Compared with CoHCF, the PANI–CoHCF composites facilitate the lattice water removal and construct excellent electron conductive networks, thereby significantly improving the specific capacitance, power density, and energy density. Compared with pure PANI, the as-prepared composite can increase the effective electrochemically active surface area of PANI and inhibit the capacitance decay caused by structural collapse/swelling. Therefore, we believe that this kind of ZHSC based on conductive polymers and PBA composite material is highly promising in practical application scenarios, and further exploration will be meaningful.

Supporting Information

Supporting Information is available from the Wiley Online Library or from the author.

Conflict of Interest

The authors declare no conflict of interest.

Data Availability Statement

The data that support the findings of this study are available from the corresponding author upon reasonable request.

[1] H. Dong, J. Li, J. Guo, F. Lai, F. Zhao, Y. Jiao, D. J. L. Brett, T. Liu, G. He, I. P. Parkin, *Adv. Mater.* **2021**, *33*, 2007548.

[2] Y. Lan, Y. Liu, J. Li, D. Chen, G. He, I. P. Parkin, *Adv. Sci.* **2021**, *8*, 2004036.

[3] J. Li, K. McColl, X. Lu, S. Sathasivam, H. Dong, L. Kang, Z. Li, S. Zhao, A. G. Kafizas, R. Wang, D. J. L. Brett, P. R. Shearing, F. Corà, G. He, C. J. Carmalt, I. P. Parkin, *Adv. Energy Mater.* **2020**, *10*, 2000058.

[4] Y. Liu, G. He, H. Jiang, I. P. Parkin, P. R. Shearing, D. J. L. Brett, *Adv. Funct. Mater.* **2021**, *31*, 2010445.

[5] H. Dong, J. Li, S. Zhao, F. Zhao, S. Xiong, D. J. L. Brett, G. He, I. P. Parkin, *J. Mater. Chem. A* **2020**, *8*, 22637.

[6] X. Guo, Z. Zhang, J. Li, N. Luo, G.-L. Chai, T. S. Miller, F. Lai, P. Shearing, D. J. L. Brett, D. Han, Z. Weng, G. He, I. P. Parkin, *ACS Energy Lett.* **2021**, *6*, 395.

[7] Y. Shao, M. F. El-Kady, J. Sun, Y. Li, Q. Zhang, M. Zhu, H. Wang, B. Dunn, R. B. Kaner, *Chem. Rev.* **2018**, *118*, 9233.

[8] Y. Liu, P. R. Shearing, G. He, D. J. L. Brett, in *Advances in Sustainable Energy* (Eds: Yj. Gao, W. Song, J. L. Liu, S. Bashir), Springer, Cham **2021**, pp. 417–449, https://doi.org/10.1007/978-3-030-74406-9_15.

[9] Y. Tian, R. Amal, D.-W. Wang, *Front. Energy Res.* **2016**, *4*, 34.

[10] Y. Liu, X. Lu, F. Lai, T. Liu, P. R. Shearing, I. P. Parkin, G. He, D. J. L. Brett, *Joule* **2021**, *5*, 2845.

[11] S. Xu, C. Su, T. Wang, Y. Ma, J. Hu, J. Hu, N. Hu, Y. Su, Y. Zhang, Z. Yang, *Electrochim. Acta* **2018**, *259*, 617.

[12] R. Liu, S. Xu, X. Shao, Y. Wen, X. Shi, J. Hu, Z. Yang, *Nanotechnology* **2021**, *32*, 502004.

[13] Q. Chen, J. Jin, M. Song, X. Zhang, H. Li, J. Zhang, G. Hou, Y. Tang, L. Mai, L. Zhou, *Adv. Mater.* **2022**, *34*, 2107992.

[14] Q. Chen, J. Jin, Z. Kou, C. Liao, Z. Liu, L. Zhou, J. Wang, L. Mai, *Small* **2020**, *16*, 2000091.

[15] Y. Jiao, L. Kang, J. Berry-Gair, K. McColl, J. Li, H. Dong, H. Jiang, R. Wang, F. Corà, D. J. L. Brett, G. He, I. P. Parkin, *J. Mater. Chem. A* **2020**, *8*, 22075.

[16] Y. Lu, Z. Li, Z. Bai, H. Mi, C. Ji, H. Pang, C. Yu, J. Qiu, *Nano Energy* **2019**, *66*, 104132.

[17] S. Wu, Y. Chen, T. Jiao, J. Zhou, J. Cheng, B. Liu, S. Yang, K. Zhang, W. Zhang, *Adv. Energy Mater.* **2019**, *9*, 1902915.

[18] G. Z. Chen, *Int. Mater. Rev.* **2017**, *62*, 173.

[19] H. Wang, Q. Hao, X. Yang, L. Lu, X. Wang, *Electrochem. Commun.* **2009**, *11*, 1158.

[20] H. Wang, J. Lin, Z. X. Shen, *J. Sci. Adv. Mater. Dev.* **2016**, *1*, 225.

[21] C. A. Amarnath, S. N. Sawant, *Electrochim. Acta* **2019**, *295*, 294.

[22] D. S. Kim, H. Yoo, M. S. Park, H. Kim, *J. Alloys Compd.* **2019**, *791*, 385.

[23] Z. Liu, G. Pulletikurthi, F. Endres, *ACS Appl. Mater. Interfaces* **2016**, *8*, 12158.

[24] Q. Xue, L. Li, Y. Huang, R. Huang, F. Wu, R. Chen, *ACS Appl. Mater. Interfaces* **2019**, *11*, 22339.

[25] B. Wang, Y. Han, X. Wang, N. Bahlawane, H. Pan, M. Yan, Y. Jiang, *iScience* **2018**, *3*, 110.

[26] R. Bai, P. Chen, S. Zeng, Y. Zhou, W. Nie, Y. Xu, *Int. J. Energy Res.* **2021**, *45*, 14870.

[27] Y. Wang, X. Jia, M. Zhu, X. Liu, D. Chao, *New J. Chem.* **2020**, *44*, 8138.

[28] J. Huang, Z. Wang, M. Hou, X. Dong, Y. Liu, Y. Wang, Y. Xia, *Nat. Commun.* **2018**, *9*, 2906.

[29] D. Yang, J. Xu, X. Z. Liao, H. Wang, Y. S. He, Z. F. Ma, *Chem. Commun.* **2015**, *51*, 8181.

[30] A. Chellachamy Anbalagan, S. N. Sawant, *Polymer* **2016**, *87*, 129.

[31] B. Thakur, S. N. Sawant, *Chempluschem* **2013**, *78*, 166.